Available online at www.sciencedirect.com
ScienceDirect
International Communications in Heat and Mass Transfer 34 (2007) 534–543
International Communications in HEAT and MASS TRANSFER
www.elsevier.com/locate/ichmt

Nanoparticle-enhanced phase change materials (NEPCM) with great potential for improved thermal energy storage ☆

J.M. Khodadadi *, S.F. Hosseinizadeh [1]

Department of Mechanical Engineering, Auburn University, 270 Ross Hall, Auburn University, Alabama 36849-5341, USA

Available online 26 March 2007

Abstract

Improved functionality of phase change materials (PCM) through dispersion of nan oparticles is reported. The resulting nanoparticle-enhanced phase change materials (NEPCM) exhibit enhanced thermal conductivity in comparison to the base material. Starting with steady state natural convection within a differentially-heated square cavity that contains a nanofluid (water plus copper nanoparticles), the nanofluid is allowed to undergo solidification. Partly due to increase of thermal conductivity and also lowering of the latent heat of fusion, higher heat release rate of the NEPCM in relation to the conventional PCM is observed. The predicted increase of the heat release rate of the NEPCM is a clear indicator of its great potential for diverse thermal energy storage applications.

Keywords: Nanoparticles; Nanofluids; Phase change; Thermal storage; Natural convection; Freezing

1. Introduction

Utilization of naturally-occurring or fabricated nanoparticles (diameters less than 50 nm) promises to open up a great number of opportunities for new technological innovations in materials synthesis, biotechnology, deep space exploration, design of microfluidic devices, emission control and energy efficiency. Masuda et al. [1] reported on enhanced thermal conductivity of dispersed ultra-fine (nanosize) particles in liquids. Soon thereafter, Choi [2] was the first to coin the term "nanofluids" for this new class of fluids with superior thermal properties. Another opportunity that has been overlooked is the exploitation of the thermal properties of nanomaterials in preparation, tailoring and development of functionality-tested nanoparticle-enhanced phase change materials (NEPCM) through dispersion of nanoparticles. In this communication, early results of an ongoing computational/experimental study that highlights the superiority of NEPCM for thermal energy storage applications are presented.

2. Problem statement

The analysis was carried out in two separate but related stages. Firstly, steady-state buoyancy-driven convection in a differentially-heated cavity containing a nanofluid was studied, very similar to the recent work of Khanafer et al. [3].

☆ Communicated by W.J. Minkowycz.

* Corresponding author.
E-mail address: khodajm@auburn.edu (J.M. Khodadadi).
[1] Visiting Research Scholar; PhD Candidate in the Department of Aerospace Engineering, Sharif University of Technology, I. R. Iran.

0735-1933/$ - see front matter © 2007 Elsevier Ltd. All rights reserved.
doi:10.1016/j.icheatmasstransfer.2007.02.005

Nomenclature

d_p	diameter of spherical nanoparticles, m
k	thermal conductivity, W/mK
L	latent heat of fusion, J/kg
Ste	Stefan number, i.e. $c_p \Delta T/L$

Greek symbols

ϕ	volume fraction of solid particles
λ	volume fraction of the nanofluid
τ	freezing time, s

Subscripts

f	base fluid
nf	nanofluid
s	solid
0	stagnant
1, 2	related to Grashof numbers 10^4 and 10^5, respectively

Consider a differentially-heated square cavity (side H) with adiabatic top and bottom walls, whereas the left and right walls are maintained at constant temperatures, T_H and T_C ($T_C < T_H$), respectively. Gravity acts parallel to the active walls pointing toward the bottom wall. The nanofluid is treated as an incompressible and Newtonian fluid. Thermophysical properties of the nanofluid are assumed to be constant, whereas the density variation in the buoyancy force term is handled by the Boussinesq approximation.

2.1. Governing relations

Considering the nanofluid as a continuous media with thermal equilibrium between the base fluid and the solid nanoparticles, the governing equations are:

Continuity:

$$\frac{\partial u}{\partial x} + \frac{\partial v}{\partial y} = 0, \tag{1}$$

X-momentum equation:

$$\frac{\partial u}{\partial t} + u\frac{\partial u}{\partial x} + v\frac{\partial u}{\partial y} = \frac{1}{\rho_{nf}}\left(-\frac{\partial p}{\partial x} + \mu_{nf}\nabla^2 u + (\rho\beta)_{nf}\, g_x(T - T_{ref})\right), \tag{2}$$

Y-momentum equation:

$$\frac{\partial v}{\partial t} + u\frac{\partial v}{\partial x} + v\frac{\partial v}{\partial y} = \frac{1}{\rho_{nf}}\left(-\frac{\partial p}{\partial y} + \mu_{nf}\nabla^2 v + (\rho\beta)_{nf}\, g_y(T - T_{ref})\right), \tag{3}$$

Energy equation:

$$\frac{\partial T}{\partial t} + u\frac{\partial T}{\partial x} + v\frac{\partial T}{\partial y} = \frac{\partial}{\partial x}\left[\frac{(k_{nf0} + k_d)}{(\rho c_p)_{nf}}\frac{\partial T}{\partial x}\right] + \frac{\partial}{\partial y}\left[\frac{(k_{nf0} + k_d)}{(\rho c_p)_{nf}}\frac{\partial T}{\partial y}\right]. \tag{4}$$

The density of the nanofluid is given by:

$$\rho_{nf} = (1-\phi)\rho_f + \phi\rho_s, \tag{5}$$

whereas the heat capacitance of the nanofluid and part of the Boussinesq term are:

$$(\rho c_p)_{nf} = (1-\phi)(\rho c_p)_f + \phi(\rho c_p)_s, \tag{6}$$

$$(\rho\beta)_{nf} = (1-\phi)(\rho\beta)_f + \phi(\rho\beta)_s, \tag{7}$$

with ϕ being the volume fraction of the solid particles and subscripts f, nf and s stand for base fluid, nanofluid and solid, respectively. The viscosity of the nanofluid containing a dilute suspension of small rigid spherical particles is given by:

$$\mu_{nf} = \frac{\mu_f}{(1-\phi)^{2.5}}, \tag{8}$$

whereas the thermal conductivity of the stagnant (subscript 0) nanofluid is:

$$\frac{k_{nf0}}{k_f} = \frac{k_s + 2k_f - 2\phi(k_f - k_s)}{k_s + 2k_f + \phi(k_f - k_s)}. \tag{9}$$

The effective thermal conductivity of the nanofluid is:

$$k_{eff} = k_{nf0} + k_d, \tag{10}$$

and the thermal conductivity enhancement term due to thermal dispersion is given by:

$$k_d = C(\rho c_p)_{nf}\sqrt{u^2 + v^2}\phi d_p. \tag{11}$$

The empirically-determined constant C is evaluated following the work of Wakao and Kaguei [4].

2.2. Buoyancy-driven convection of nanofluid

Taking the lower left corner of the cavity as the origin of the coordinate system, $g_x = 0$ and $g_y = -g$. The above relations are identical to the work of Khanafer et al. [3], thus allowing us to benchmark our computer code by comparing our findings to theirs. The particular nanofluid of interest was that of solid copper nanoparticles ($d_p = 10$ nm) suspended in water as the base fluid. Temperature difference of the two walls was 10 °C ($T_H = 283.15$ and $T_C = 273.15$ K). The pertinent thermophysical properties are given in Table 1 that were taken from Khanafer et al. [3]. The boundary conditions are:

$$\begin{aligned}
&u = v = \frac{\partial T}{\partial y} = 0 && \text{at } y = 0, H && \text{and } 0 \le x \le H,\\
&u = v = 0, T = T_H && \text{at } x = 0 && \text{and } 0 \le y \le H,\\
&u = v = 0, T = T_C && \text{at } x = H && \text{and } 0 \le y \le H.
\end{aligned} \tag{12}$$

2.3. Modeling of freezing of the NEPCM

Starting at time $t = 0$, the temperatures of both active left and right walls were lowered by the same amount such that the cold right wall was held 10 °C below the freezing temperature of the base fluid. Consequently, the nanofluid will start freezing on the right wall and the solid front travels to the left. The remaining boundary conditions were unchanged in comparison to the conditions prior to $t = 0$.

Table 1
Thermophysical properties of the copper nanoparticles, water ($\phi=0$) and nanofluids with solid copper nanoparticle volume fractions (ϕ) equal to 0.1 and 0.2

	Copper nanoparticles	Base fluid	Nanofluid 1	Nanofluid 2
		$\phi=0$	$\phi=0.1$	$\phi=0.2$
ρ [kg/m^3]	8954	997.1	1792.79	2588.48
μ [Pa s]	–	8.9×10^{-4}	1.158×10^{-3}	1.555×10^{-3}
c_p [J/kg K]	383	4179	2283.107	1552.796
k [W/m K]	400	0.6	0.8	1.04748
α [m^2/s]	1.17×10^{-4}	1.44×10^{-7}	1.95×10^{-7}	2.6×10^{-7}
β [1/K]	1.67×10^{-5}	2.1×10^{-4}	1.13×10^{-4}	7.63×10^{-5}
L [J/kg]	–	3.35×10^{5}	1.68×10^{5}	1.03×10^{5}
Pr	–	6.2	3.31	2.3
Ste	–	0.125	0.136	0.150
τ_1 [s]	–	2950	2000	1300
τ_2 [s]	–	3000	2000	1400

2.4. Computational methodology

The SIMPLE method within version 6.2.16 of the commercial code FLUENT [5] was utilized for solving the governing equations. For all the cases reported here, uniform grid spacings for both x and y directions were utilized. The time step for integrating the temporal derivatives was set to 1 s. The QUICK differencing scheme was used for solving the momentum and energy equations, whereas the PRESTO scheme was adopted for the pressure correction equation. The under-relaxation factors for the velocity components, pressure correction, thermal energy and liquid fraction were 0.5, 0.3, 1 and 0.9, respectively. In order to satisfy convergence criteria (10^{-7} for continuity and momentum, and 10^{-9} for thermal energy), the number of iterations for every time step was between 400 and 700. A single-domain enthalpy–porosity formulation that treats different phases as porous media was utilized. In effect, Darcy Law damping terms of the form $\frac{A(1-\lambda)^2}{\lambda^3}v_i$ with $i=x$ and y were added to the momentum equations. The term λ stands for the nanofluid volume fraction at a given point that is equal to unity for the fluid phase, whereas it becomes zero upon freezing. The mushy zone constant (A) was set to 10^5 kg/m^{3}s. The enthalpy of the material is composed of the sensible enthalpy and the latent heat of fusion. The latent heat that is evaluated using:

$$(\rho L)_{nf} = (1-\phi)(\rho L)_f, \tag{13}$$

is liberated proportionately to the nanofluid volume fraction that is defined using a lever rule between the liquidus and solidus temperatures. Theoretical details of these techniques can be found elsewhere (Voller and Prakash [6], Khodadadi and Zhang [7] and FLUENT [5]).

3. Benchmarking of the models

The predicted progress of the melt front with time as reported by Brent et al. [8] and measured by Gau and Viskanta [9] are compared to the present computed data in Fig. 1. Brent et al. [8] considered melting of a solid material contained in a rectangular enclosure with insulated top and bottom walls. The qualitative trends among the three approaches are agreeable, whereas the present computations suggest a greater role for natural convection indicated by the uneven melting in the top half of the cavity compared to the bottom half.

The results of the recent work of Khanafer et al. [3] were used to benchmark the present computations for the case of natural convection of nanofluids within a differentially-heated square cavity. The predicted horizontal velocity component on the vertical mid-plane of the square cavity for the present study with a 81×81 grid system and that of Khanafer et al. [3] are compared in Fig. 2 for $Gr=10^4$ and 10^5. Regardless of the volume fraction of the nanoparticles, the well-established trends of the horizontal fluid velocity exhibiting accelerated flow near the horizontal walls and weak flow in the center of the cavity point to the observation that nanofluids behave more like

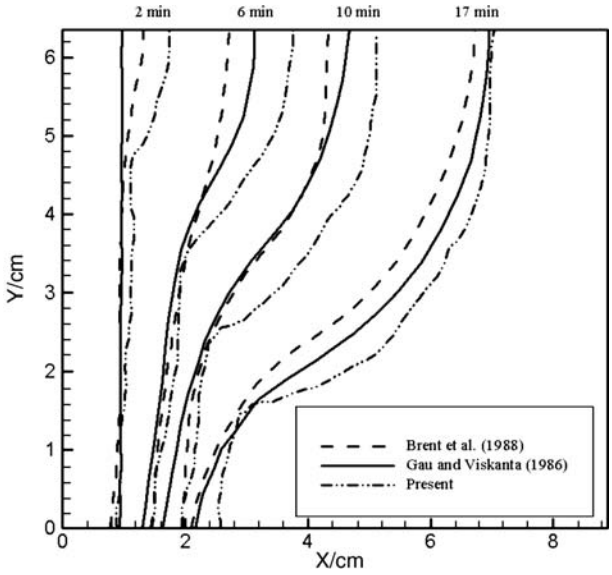

Fig. 1. Progress of the melt front with time: Comparison among the predictions of Brent et al. [8], present work (42 × 32 grid) and experimental data of Gau and Viskanta [9].

a fluid (Khanafer et al. [3]) as opposed to flow of mm- or micron-size suspensions. The comparison for the cases of buoyancy-driven convection of a pure fluid (zero volume fraction) for the two Grashof numbers is excellent. According to Khanafer et al. [3], the dimensionless velocity was related to the inverse of the temperature difference between the two active walls. Consequently, the dimensionless velocity for $Gr=10^5$ is lower compared to the corresponding $Gr=10^4$ case. For a fixed Grashof number, as the loading of the nanoparticles is increased, "irregular and random" (Khanafer et al. [3]) motion of the nanoparticles promote greater momentum and energy transport throughout the cavity. Consequently, the extra thermal conductivity due to dispersion is enhanced. It should be noted that in the study of Khanafer et al. [3], both the Prandtl and Grashof numbers were evaluated using the properties of the base fluid. In our work, these dimensionless groupings were evaluated using the properties of

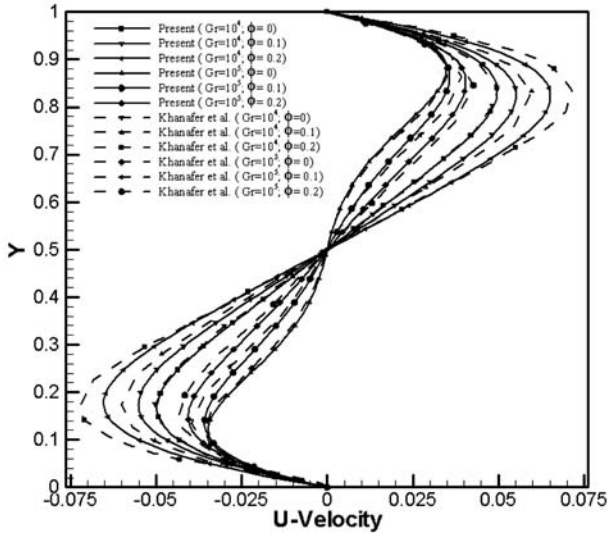

Fig. 2. Comparison of the predicted horizontal velocity component on the vertical mid-plane of the square cavity for the present study and those of Khanafer et al. [3] with $Gr=10^4$ and 10^5.

the specific nanofluids. In effect, it appears that there are discrepancies between our predictions and those of Khanafer et al. [3] for nonzero solid volume fractions. The reader should not be alarmed on this matter in view of the different scaling parameters used to form the dimensionless groupings.

4. Freezing of the NEPCM

Improved functionality of nanoparticle-enhanced phase change materials (NEPCM) compared to the base fluid is the centerpiece of this communication. Starting with steady natural convection within a water–copper nanofluid that is inside a differentially-heated square cavity, freezing of the NEPCM was investigated. The temperatures of the left and right walls were lowered by 10 °C. In effect, the cold right wall was held 10 °C lower than the freezing temperature of the base fluid (273.15 K). Consequently, the nanofluid will start freezing on the right wall and

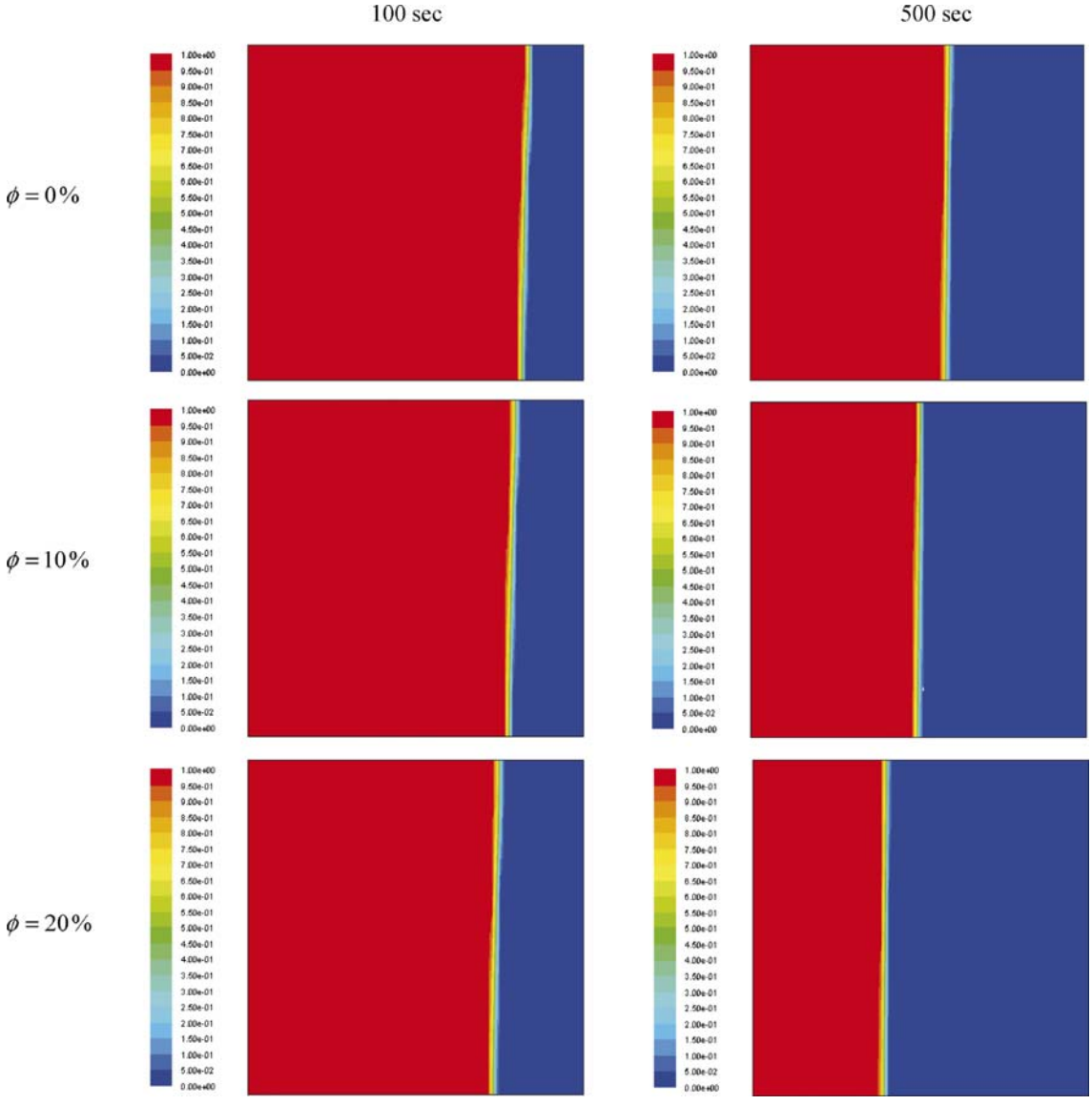

Fig. 3. Colorized contours of the volume fraction of the nanofluid (λ) at various time instants during the freezing of water with copper nanoparticles for an initial $Gr = 10^4$ (solid particle volume fractions of 0, 0.1 and 0.2 and $Ste = 0.125$, 0.136 and 0.150, respectively). (For interpretation of the references to colour in this figure legend, the reader is referred to the web version of this article.)

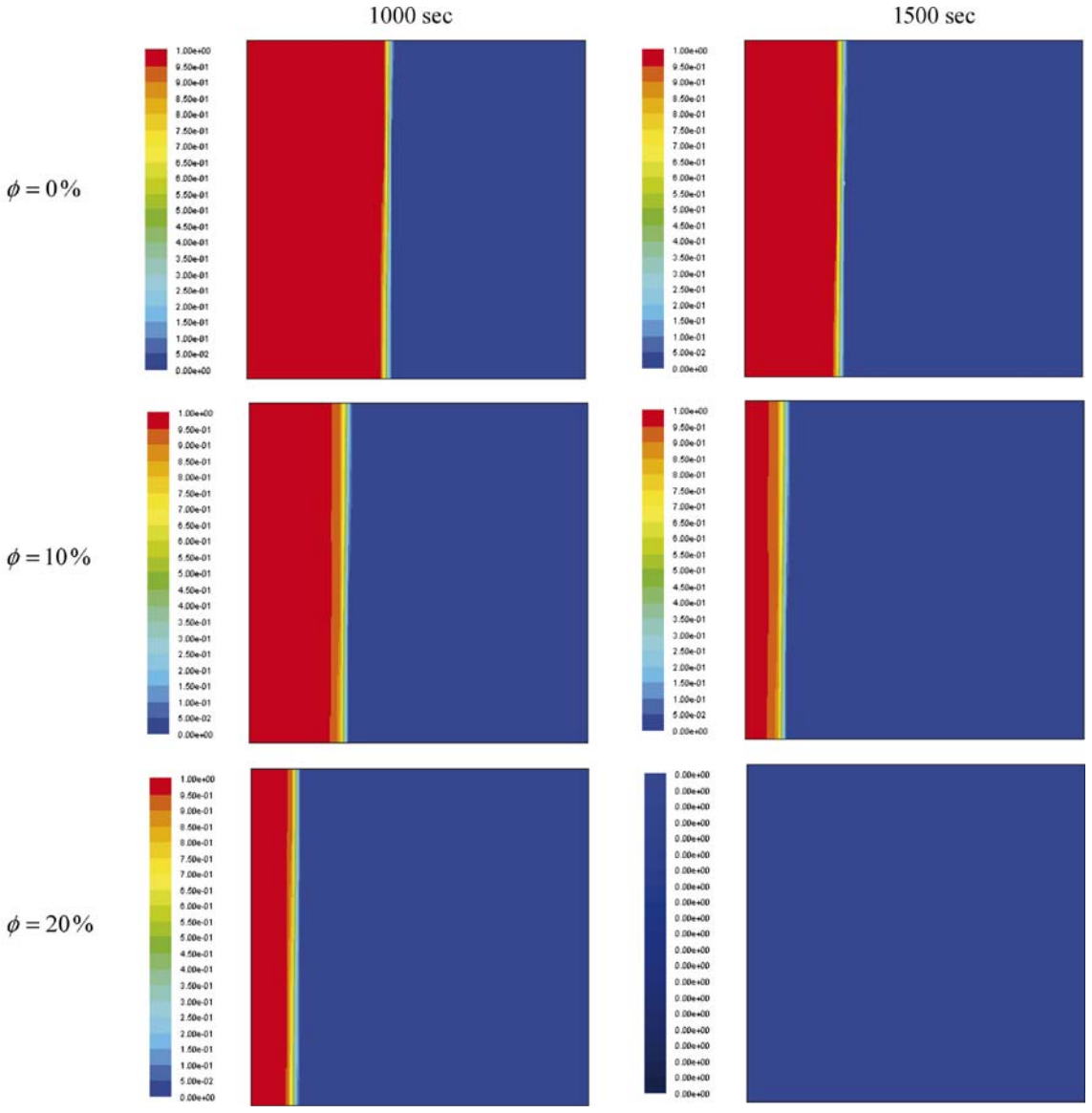

Fig. 3 (*continued*).

the solid front travels to the left. The other boundary conditions remained unchanged. Three solid particle volume fractions of 0, 0.1 and 0.2 were considered for two initial Grashof numbers of 10^4 and 10^5. The pertinent properties are given in Table 1 and the corresponding Stefan numbers for the three solid particle volume fractions of 0, 0.1 and 0.2 were 0.125, 0.136 and 0.150, respectively. Colorized contours of the volume fraction of the nanofluid, i.e. λ (0 and 1 for solid and liquid phases, respectively) during freezing of the NEPCM at various time instants are shown in Fig. 3 for an initial Grashof number of 10^4. The time instants in Fig. 3 are 100, 500, 1000 and 1500 s. Color red is used to identify the liquid phase, whereas color blue is indicative of the frozen solid phase. In general, the sharp liquid–solid interface is nearly vertical with a mild misalignment toward the colder wall early on, thus favoring a longer wetted length on the top insulated wall. This can be attributed to the buoyancy-driven convection in the cavity that was already at full strength at $t=0$ in the form of a clockwise (CW) rotating vortex. For $t>0$, the strength of this vortex diminishes whereas a second counter-clockwise (CCW) rotating vortex is created next to the left wall (to be discussed below). Observations on the instantaneous volume of the frozen solid phase and the shape of the interface for the case of freezing of pure water ($\phi=0$) are in general agreement with findings of Banaszek et al. [10]. For this Grashof number

($Gr=10^4$), it is observed that as the solid particle volume fraction is raised, the NEPCM will freeze more rapidly. This is due to the enhanced thermal conductivity of the nanofluid and smaller value of the latent heat, to be further discussed below.

The instantaneous streamlines within the nanofluid for the initial 10 s during the freezing of NEPCM for an initial $Gr=10^5$, $Ste=0.150$ and a solid particle volume fraction of 0.2 are shown in Fig. 4. The streamlines at $t=0$ correspond to a similar case studied by Khanafer et al. [3] and a CW rotating vortex is clearly observed. As a result of the sudden lowering of the temperatures of the two active walls at $t=0$, the CW rotating vortex diminishes in strength and spatial coverage due to formation of a CCW rotating vortex next to the left wall. The creation of the dual-vortex flow pattern was examined in greater detail by lowering the time step to 0.1 s for this case. Note that the formation, growth and equilibration of the CCW vortex during the initial 10 s involves a dynamic interaction with the initially strong CW vortex. At the $t=10$ s instant, two vortices rotating in opposite directions and nearly equal in size are observed squeezed between the left wall and a thin frozen layer next to the right wall. For the remainder of the freezing process, the dual-vortex structure will persist however due to the leftward movement of the freezing front, the vortices will shrink in coverage space and their strength will decay. It should be noted that the actual Grashof number for this unsteady freezing problem decreases with time due to the continuous shrinking of the distance between the left wall and the liquid–solid interface.

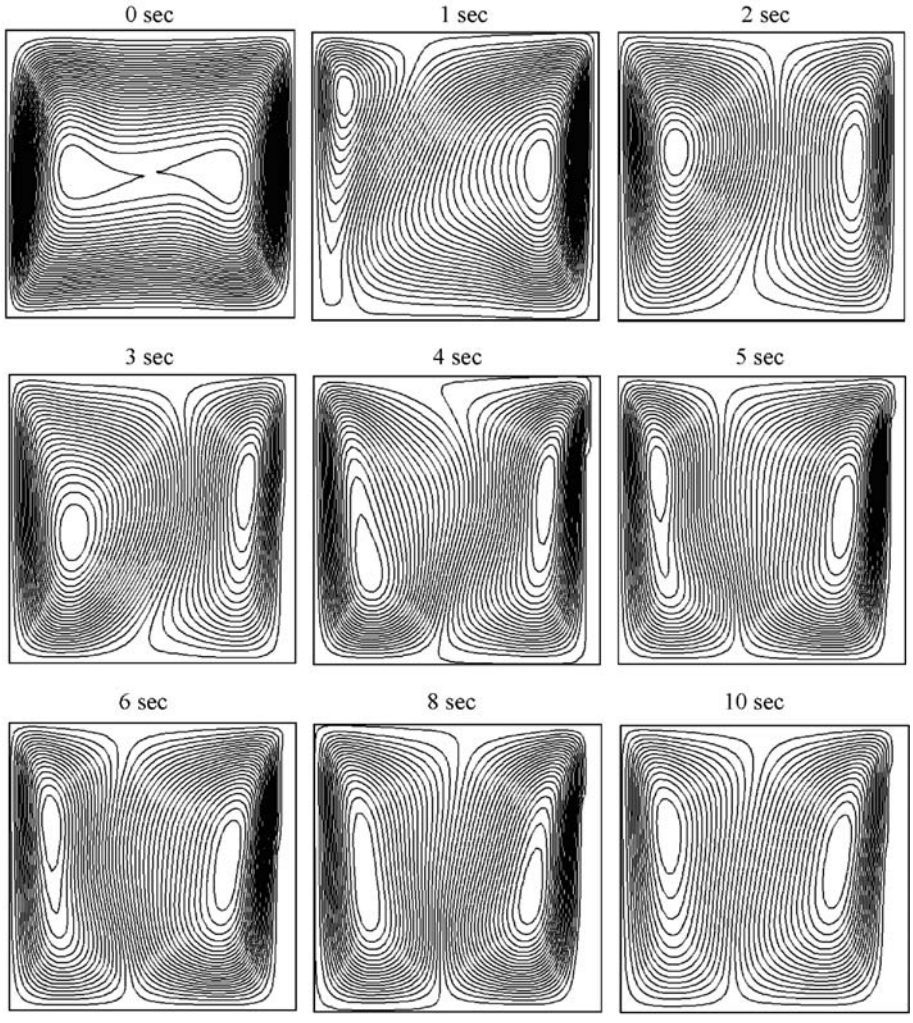

Fig. 4. Streamline patterns at various time instants for the initial 10 s during the freezing of water with copper nanoparticles (solid particle volume fraction of 0.2) for an initial $Gr=10^5$ and $Ste=0.150$.

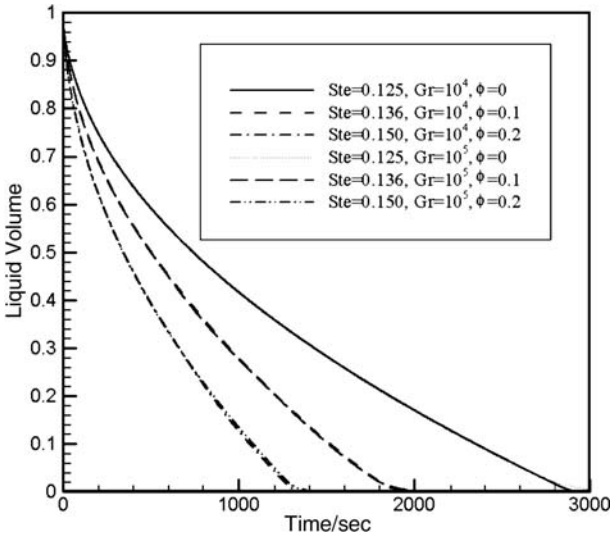

Fig. 5. Instantaneous volume of the nanofluid within the square cavity.

The instantaneous dimensionless volume of the nanofluid within the square cavity, i.e.:

$$\text{Liquid Volume}(t) = \int_{x=0}^{H} \int_{y=0}^{H} \lambda(x,y,t)\mathrm{d}x\mathrm{d}y/H^2, \tag{14}$$

is presented in Fig. 5 for all the cases that were investigated. The liquid volume that continuously decreases from the start of the freezing exhibits little sensitivity to the value of the initial Grashof number except near the conclusion of the freezing process. On the other hand, the volume of the nanofluid is strongly dependent on the solid particle volume fraction of the dispersed nanoparticles. The freezing times for pure water and copper–water nanofluids for initial Grashof numbers of 10^4 and 10^5 are summarized in Table 1. For a given initial Grashof number, as the solid particle volume fraction is raised the freezing time is lowered. This is due to the enhanced thermal conductivity of the nanofluid in comparison to that of the base liquid. At the same time, due to lowering of the latent heat of fusion, less energy per unit mass of the nanofluid is needed for freezing this specific NEPCM. The observed higher heat release rate of the NEPCM is a clear indicator of its great potential for thermal energy storage applications.

5. Conclusions

Given proper suspension of nanoparticles within conventional phase change materials such as water, it is shown that NEPCM have great potential for demanding thermal energy storage applications. Specifically, the high heat release rate of the NEPCM in relation to the conventional PCM and its higher thermal conductivity point to its promise for greater utilization in diverse energy sectors.

Acknowledgement

The second author (SFH) acknowledges the support of the Ministry of Science, Research and Technology of the I. R. Iran through a short-term scholarship.

References

[1] H. Masuda, A. Ebata, K. Teramae, N. Hishinuma, Alteration of thermal conductivity and viscosity of liquid by dispersing ultra-fine particles, Netsu Bussei 7 (4) (1993) 227–233.

[2] U.-S. Choi, Enhancing thermal conductivity of fluids with nanoparticles, in: Developments and Application of Non-Newtonian Flows, ASME, FED-Vol. 231/MD-Vol. 66, 1995, pp. 99–105.
[3] K. Khanafer, K. Vafai, M. Lightstone, Buoyancy-driven heat transfer enhancement in a two-dimensional enclosure utilizing nanofluids, Int. J. Heat Mass Transfer 46 (19) (2003) 3639–3653.
[4] N. Wakao, S. Kaguei, Heat and Mass Transfer in Packed Beds, Gordon and Breach Science Publishers, New York, 1982, pp. 175–205.
[5] FLUENT 6.1 User's Guide, Fluent, Inc., Lebanon, NH, 2003.
[6] V.R. Voller, C. Prakash, A fixed-grid numerical modeling methodology for convection–diffusion mushy region phase-change problems, Int. J. Heat Mass Transfer 30 (8) (1987) 1709–1719.
[7] J.M. Khodadadi, Y. Zhang, Effects of buoyancy-driven convection on melting within spherical containers, Int. J. Heat Mass Transfer 44 (8) (2001) 1605–1618.
[8] A.D. Brent, V.R. Voller, K.J. Reid, Enthalpy–porosity technique for modeling convection–diffusion phase change: application to the melting of a pure metal, Numer. Heat Transf. 13 (3) (1988) 297–318.
[9] C. Gau, R. Viskanta, Melting and solidification of a pure metal on a vertical wall, J. Heat Transfer 108 (1) (1986) 174–181.
[10] J. Banaszek, Y. Jaluria, T.A. Kowalewski, M. Rebow, Semi-implicit FEM analysis of natural convection in freezing water, Numer. Heat Transf. A 36 (5) (1999) 449–472.